Particle-in-cell simulations of fast magnetic field penetration into plasmas due to the Hall electric field

S. B. Swanekamp,[a] J. M. Grossmann, A. Fruchtman,[b] B. V. Oliver,[c] and P. F. Ottinger
Plasma Physics Division, Naval Research Laboratory, Washington, D.C. 20375

(Received 30 March 1996; accepted 25 June 1996)

Particle-in-cell (PIC) simulations are used to study the penetration of magnetic field into plasmas in the electron-magnetohydrodynamic (EMHD) regime. These simulations represent the first definitive verification of EMHD with a PIC code. When ions are immobile, the PIC results reproduce many aspects of fluid treatments of the problem. However, the PIC results show a speed of penetration that is between 10% and 50% slower than predicted by one-dimensional fluid treatments. In addition, the PIC simulations show the formation of vortices in the electron flow behind the EMHD shock front. The size of these vortices is on the order of the collisionless electron skin depth and is closely coupled to the effects of electron inertia. An energy analysis shows that one-half the energy entering the plasma is stored as magnetic field energy while the other half is shared between internal plasma energy (thermal motion and electron vortices) and electron kinetic energy loss from the volume to the boundaries. The amount of internal plasma energy saturates after an initial transient phase so that late in time the rate that magnetic energy increases in the plasma is the same as the rate at which kinetic energy flows out through the boundaries. When ions are mobile it is observed that axial magnetic field penetration is followed by localized thinning in the ion density. The density thinning is produced by the large electrostatic fields that exist inside the electron vortices which act to reduce the space-charge imbalance necessary to support the vortices. This mechanism may play a role during the opening process of a plasma opening switch. [S1070-664X(96)00610-6]

I. INTRODUCTION

Magnetic field penetration into plasma is one of the most fundamental issues studied in plasma physics. Although the results of this paper are presented in the context of the plasma-opening switch (POS),[1,2] the results have a wide range of other applications including space plasmas,[3] fast Z pinches,[4] charged particle beam propagation in plasmas,[5,6] and basic laboratory experiments.[7] Much of the early work on this subject was performed within the realm of magnetohydrodynamic (MHD) theory where ions move under the influence of $J\times B$ forces and the magnetic field is convected with the ion fluid.[8] In this case, the characteristic ion speed is given by the Alfvén speed, $V_A=B/(4\pi n_i m_i)^{1/2}$, where B is the magnetic field strength, n_i is the ion density, and m_i is the ion mass. If the plasma is collisional, a magnetic field can penetrate due to resistive diffusion at a rate given by $V_D=c^2\eta/(4\pi L_D)$, where c is the speed of light, η is the resistivity (arising from either classical or anomalous collisions), and L_D is the characteristic diffusion length.[9] Recent theoretical studies have shown that the magnetic field can penetrate into initially unmagnetized plasma on a time scale faster than either the Alfvén speed or resistive diffusion.[10] This penetration results from the addition of the Hall electric field in Ohm's law in ideal MHD theory. In this case the magnetic field is convected with the electron fluid with a characteristic speed given by $V_H=cB/(4\pi n_e e L_H)$, where n_e is the electron density, e is the magnitude of the electron charge, and L_H is the characteristic scale length for Hall penetration. The ratio of the Alfvén speed to the Hall speed can be written as $V_A/V_H=L_H/(c/\omega_{pi})$, where $\omega_{pi}=(4\pi Z n_i e^2/m_i)^{1/2}$ is the ion plasma frequency and c/ω_{pi} is the collisionless ion skin depth. Therefore, Hall penetration is faster than magnetic field convection due to ion motion when the characteristic Hall length is small compared with the ion collisionless skin depth. Similarly, it can be shown that Hall penetration is faster than resistive diffusion provided $\nu<\Omega_\theta L_D/L_H$ where ν is the collision frequency, $\Omega_\theta=eB_\theta/m_e c$ is the electron cyclotron frequency, and m_e is the electron rest mass.

This paper presents the first verification of Hall penetration using the particle-in-cell (PIC) method.[11] The simulations are performed using the MAGIC code developed at Mission Research Corporation.[12] Many of the earlier studies of Hall penetration were performed with a fluid approach using various approximations.[13–16] Some of the approximations that are necessary to close the fluid equations, such as the form for the pressure tensor and the equation of state, make solutions of the fluid equations questionable. In addition, much of the past work required a small amount of collisionality to remove singularities. However, even this small amount of collisionality can lead to difficulties. For example, a small amount of collisionality can lead to unphysically large plasma heating for the drive currents expected in a POS. The PIC method can provide answers to these questions since it is a collisionless, kinetic approach, that requires no assumptions regarding the pressure tensor or plasma equation of state. When there are no collisions, it would be

[a]JAYCOR, Vienna, Virginia 22812. Electronic mail: swane@calvin.nrl.navy.mil
[b]Science Applications International Corporation, McLean, Virginia 22102 and Princeton Plasma Physics Laboratory, Princeton, New Jersey 08543.
[c]National Research Council Research Associate at the Naval Research Laboratory.

 1070-664X/96/3(10)/3556/8/$10.00

interesting to understand how energy is partitioned between magnetic field energy and internal plasma energy.

Previous PIC simulations of gap formation in the POS have shown evidence of magnetic field penetration and vortices in the electron flow during the gap formation process.[17] However, because several competing mechanisms associated with ion motion occur simultaneously, it has been difficult to verify that this penetration is connected to the Hall effect. Vortices in the electron flow have also been predicted analytically[18–21] and observed with the two fluid code ANTHEM.[22]

The PIC results presented in this paper show that vortices in the electron flow accompany magnetic field penetration and these vortices are a natural consequence of the electron inertia. These vortices are similar in many aspects to the vortices observed in PIC simulations of vacuum electron flow in magnetically insulated transmission lines (MITLs).[23] Much of the theory developed in Sec. II applies to vacuum flow in MITLs as well.

The outline of the paper is as follows. In Sec. II a brief discussion of the fluid treatment of Hall penetration is presented as well as some of the key results from the fluid approach. In Sec. III results are presented from several PIC simulations that show magnetic field penetration into the plasma. It is shown that the observed penetration agrees very well with the fluid description in many aspects. However, the PIC simulations also show paramagnetic vortices in the electron flow and the penetration speed is slower than that predicted by the fluid theory. Section IV presents a detailed discussion of the partition of energy in the plasma between magnetic energy, thermal and directed electron energy, and energy loss to the boundaries. Because the main concern of the paper is the regime where Hall penetration dominates ($L_H \ll c/\omega_{pi}$), the ion mass is taken to be infinite for much of the paper. However, the role of ion motion is addressed in Sec. III by comparing simulation results for a case where ions can move with the case where ion mass is infinite.

II. FLUID THEORY OF MAGNETIC FIELD PENETRATION INTO PLASMAS DUE TO THE HALL ELECTRIC FIELD

In this section, the theory of magnetic field penetration into a plasma is presented using a fluid approach. To get a solution to these equations it is necessary to make several assumptions regarding the form of the pressure tensor, the role of displacement current, and the importance of electron inertia. As the basic equations for magnetic field penetration are developed, the key assumptions of the fluid approach are highlighted and compared with the physics contained in the PIC approach. In addition, the main results of the fluid theory are developed for comparison with the PIC simulations presented in the next section.

The geometry considered in this paper is that of the plasma opening switch shown in Fig. 1. A plasma of axial length l is placed between the anode and cathode of a coaxial transmission line. Current (I_G) is driven through the plasma in the form of a transverse electromagnetic (TEM) wave that is applied from the left boundary. In the analysis presented

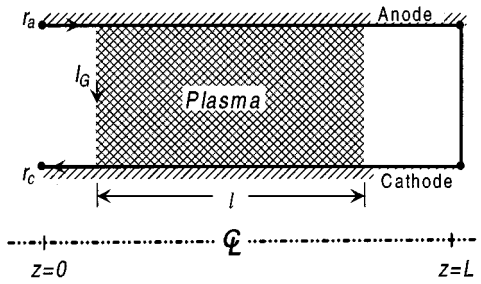

FIG. 1. The geometry used in the simulations is that of the plasma opening switch.

below azimuthal symmetry is assumed and only the TM mode set is retained with field components $E_r(r,z,t)$, $E_z(r,z,t)$, and $B_\theta(r,z,t)$.

The evolution of the electron fluid is governed by the continuity and momentum balance equations which are given by

$$\frac{\partial n_e}{\partial t} + \nabla \cdot n_e \mathbf{V}_e = 0, \tag{1}$$

$$\frac{\partial \gamma \mathbf{V}_e}{\partial t} + \mathbf{V}_e \cdot \nabla \gamma \mathbf{V}_e = -\frac{e}{m_e}\left(\mathbf{E} + \frac{\mathbf{V}_e \times \mathbf{B}}{c}\right) - \frac{\nabla \cdot \mathbf{P}}{n_e m_e} + \frac{e}{m_e}\eta \mathbf{J}, \tag{2}$$

where $\gamma = (1 - V_e^2/c^2)^{-1/2}$ is the relativistic mass factor, $\mathbf{V}_e$ is the electron fluid velocity, $\mathbf{P}$ is the pressure tensor, and $\mathbf{J}$ is the current density. In fluid treatments it is common to neglect the off-diagonal terms in the pressure tensor and treat the pressure as a scalar. Since the PIC method allows for orbit crossings, no assumption regarding the form of the pressure tensor is needed. PIC simulations of the POS have shown that the off-diagonal terms can be important in regions of the plasma where there is magnetic field penetration.[24]

When azimuthal symmetry is assumed, Eqs. (1) and (2) can be combined with Faraday's law,

$$\nabla \times \mathbf{E} = -\frac{1}{c}\frac{\partial \mathbf{B}}{\partial t}, \tag{3}$$

to give the following equation describing the evolution of the electron fluid vorticity and magnetic field;

$$n_e r \frac{D}{Dt}\left(\frac{\omega_\theta - \Omega_\theta}{n_e r}\right) = -\left(\nabla \frac{1}{m_e n_e} \times \nabla p\right)_\theta + \frac{e}{m_e}(\nabla \times \eta \mathbf{J})_\theta. \tag{4}$$

In this last equation $D/Dt = \partial/\partial t + V_e \cdot \nabla$ is the convective derivative, p is the scalar pressure, $\Omega_\theta = eB_\theta/m_e c$ is the electron cyclotron frequency, and $\omega_\theta = (\nabla \times \gamma \mathbf{V}_e)_\theta$ is the electron fluid vorticity. If the scalar pressure is only a function of the density, then the first term on the right-hand side of Eq. (4) is zero. If collisions are also ignored, then Eq. (4) describes the constancy of $\Gamma/n_e r$ along an electron trajectory, where $\Gamma = \omega_\theta - \Omega_\theta$ is the generalized electron vorticity. For example,

the electrons in the plasma prefill are initially unmagnetized and at rest so that their initial generalized vorticity is zero. As the magnetic field penetrates into the plasma these electrons seek regions of the plasma that keep their generalized vorticity zero along their trajectory.

The appearance of vorticity in solutions to the fluid equations is a direct consequence of electron inertia. In much of the previous work on Hall theory, electron inertia is ignored. This is equivalent to assuming that electrons are $\mathbf{E}\times\mathbf{B}$ drifting and results in the neglect of the fluid vorticity ($\omega_\theta=0$) in Eq. (4). When electron inertia is ignored, Eq. (4) can be written as[25]

$$\frac{D}{Dt}\left(\frac{r\Omega_\theta}{n_e r^2}\right)=0, \tag{5}$$

where the pressure and collision terms have been dropped. Equation (4) or Eq. (5) applies regardless of the details of the ion motion. Therefore, they are appropriate not only to electron flows in plasmas but also apply to vacuum electron flows in magnetically insulated transmission lines. If there is ion motion, then the electron density will evolve in a complicated manner as ions redistribute themselves. If the electron fluid remains in quasiequilibrium, then Eq. (5) implies that the electron fluid will evolve to keep $r\Omega_\theta/n_e r^2$ constant along the electron trajectories as the ion density evolves in time.

In electron magnetohydrodynamics (EMHD) it is customary to ignore ion motion and assume that the plasma is space-charge neutral ($n_e=Zn_i$). This simplifies the fluid equations because the electron density is constant and determined by the initial ion distribution. With these assumptions, an equation describing Hall penetration can be derived by expanding the convective derivative in Eq. (5) and using Ampère's law (displacement current is neglected) to eliminate the electron fluid velocity [$\mathbf{V}_e=-(c/4\pi Zn_i e)\nabla\times\mathbf{B}$]. This equation can be written as

$$\frac{\partial B_\theta}{\partial t}-\frac{crB_\theta}{4\pi e}\left(\nabla rB_\theta\times\nabla\,\frac{1}{Zn_i r^2}\right)_\theta=0. \tag{6}$$

A stable, nonlinear solution to Eq. (6) predicts a shock wave for rB_θ which propagates along the $n_i r^2$ contours.[14,26]

As a special case of Eq. (6), consider the situation where the ion density is independent of z [i.e., $n_i(r,z)=n_i(r)$]. In this case the $Zn_i r^2$ contours are parallel to the z axis and shock propagation is expected to occur in the z direction. For this special case, Eq. (6) can be expressed as[13]

$$\frac{\partial B_\theta}{\partial t}-\frac{cB_\theta}{4\pi Zn_i eL_{\mathrm{H}}}\frac{\partial B_\theta}{\partial z}=0, \tag{7}$$

where

$$L_{\mathrm{H}}=[(1/Zn_i r^2)d(Zn_i r^2)/dr]^{-1} \tag{8}$$

is the characteristic length for Hall penetration. The penetration speed of the shock front can be expressed as[13,27]

$$V_{\mathrm{H}}(r)=\alpha\,\frac{c(-rB_\theta)}{4\pi Zn_i erL_{\mathrm{H}}}, \tag{9}$$

where α is a constant on the order of unity that depends on the time dependence for the applied current, $I_G(t)=crB_\theta(r,z=0,t)/2$. Two cases of practical importance include the constant applied current and the linearly rising current for which $\alpha=1/2$ and 3/8, respectively.

It is important to note that the magnetic field will penetrate only in regions of plasma where the Hall speed is positive. When $V_{\mathrm{H}}\leqslant 0$, Eq. (7) predicts evanescent waves that do not propagate. Furthermore, if the plasma is initially magnetized then expulsion of the magnetic field is expected in regions where $V_{\mathrm{H}}\leqslant 0$.[15,22] For a POS in negative polarity ($-rB_\theta>0$), Eq. (7) predicts magnetic field penetration in regions where $d(Zn_i r^2)/dr>0$. Exclusion of the magnetic field is expected in regions where $d(Zn_i r^2)/dr\leqslant 0$. In positive polarity ($rB_\theta>0$) the regions of penetration and exclusion are reversed. In general it can be shown that magnetic field penetration occurs in the $\mathbf{B}\times\nabla(Zn_i r^2)$ direction.[16]

III. SIMULATION RESULTS

Since Hall penetration dominates ion motion when $L_{\mathrm{H}}/(c/\omega_{pi})\ll 1$, ion motion is assumed negligible in the majority of this section by taking ions to be infinitely massive. The role of ion motion will be addressed later in this section by comparing the infinitely massive ion case with a case where the ions can move.

One of the fundamental weaknesses of the PIC method is the so-called ''grid'' instability that produces numerical plasma heating. This instability saturates when[11]

$$\lambda_{\mathrm{D}}\sim\Delta x/\pi, \tag{10}$$

where Δx is the grid size, $\lambda_{\mathrm{D}}=(k_{\mathrm{B}}T_e/4\pi n_e e^2)^{1/2}$ is the plasma Debye length, k_{B} is the Boltzmann constant, and T_e is the electron temperature. Artificial plasma heating from the grid instability severely limits the plasma densities that can be accurately simulated with the PIC method. To limit the numerical heating to 10–100 eV, grid sizes of 0.005–0.01 cm were used with plasma densities ranging between 10^{12} and 3×10^{13} cm^{-3}. For these densities the electron mass was reduced from the normal electron mass to keep the collisionless electron skin depth small compared to the dimensions of the plasma (typically a few cm). At the end of this section, it is demonstrated that the results from the reduced electron mass are equivalent to those with normal electron mass and a corresponding higher magnetic field and electron density.

The simulations presented in this section are set up as shown in Fig. 1. Space-charge-limited emission of electrons is allowed from the entire cathode surface. The emitted electrons are given an initial velocity of 10^8 cm/s. This corresponds to an initial energy of about 3 eV. Plasma is loaded between $z=2$ cm and $z=5$ cm between the cathode radius of $r_c=2.5$ cm and the anode radius of $r_a=5.0$ cm. A linearly rising current ramp with $dI_G/dt=10$ kA/ns is applied on the left-hand boundary. The electron mass used in these simulations was 1/10 the normal electron mass. Two different density profiles were used. These profiles are shown Fig. 2(a). The first profile is a parabolic density profile with the minimum density of 10^{12} cm^{-3} at $r=3.75$ cm rising to 3×10^{13} cm^{-3} at the electrodes. For this density profile the character-

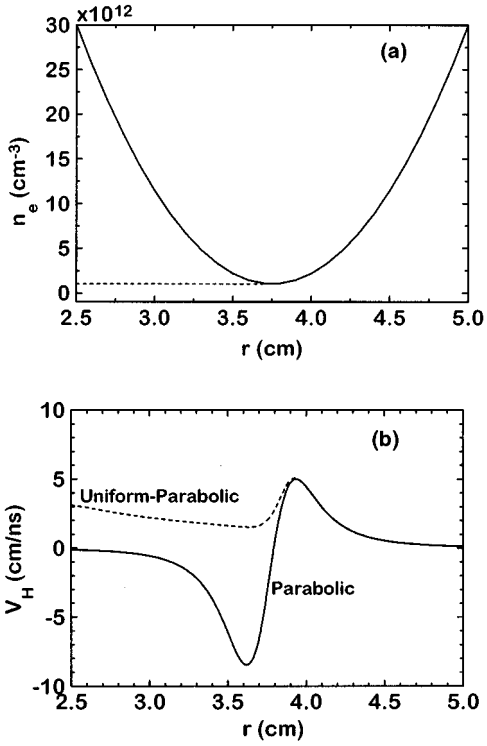

FIG. 2. (a) The parabolic and uniform-parabolic density profiles used to demonstrate EMH effects in a PIC code. (b) The Hall speed profiles in negative polarity for the density profiles shown in (a).

istic Hall scale length is 0.2 cm. The second profile is a uniform-parabolic profile that is uniform at 10^{12} cm^{-3} between the cathode and $r=3.75$ cm and then rises parabolically to 3×10^{13} cm^{-3} at the anode. The instantaneous Hall speed profiles for these two density profiles in negative polarity ($-rB_\theta>0$) are shown in Fig. 2(b). Recall from the discussion in Sec. II that magnetic field penetration is expected only in regions where the Hall speed is positive. Therefore, exclusion of the magnetic field is expected for $r\leqslant3.75$ cm in negative polarity for the parabolic profile. Magnetic field penetration is expected for $r>3.75$ cm with maximum penetration occurring near $r=4$ cm. In positive polarity the regions of penetration and exclusion are reversed. For the uniform-parabolic profile, the magnetic field is expected to penetrate the entire plasma in negative polarity. Since the regions of penetration and exclusion are reversed in positive polarity ($rB_\theta>0$), no magnetic field penetration is expected in positive polarity for the uniform-parabolic profile since the Hall speed profile is negative everywhere.

The fluid theory of Hall penetration is tested with several PIC simulations. One of the most useful diagnostics from these simulations is the contours of $rB_\theta(r,z)$. From Ampère's law, $rB_\theta(r,z)$ is proportional to the current enclosed within a radius r at axial location z. In MKS units the current enclosed is expressed as $I(r,z)=2\pi rB_\theta(r,z)/\mu_0$. With this definition, the difference between the contour levels of $I(r,z)$ represents current flow in the plasma parallel to the contours.

Current enclosed contours at $t=2$ ns are shown in Fig. 3 for the parabolic profile in negative polarity. As predicted,

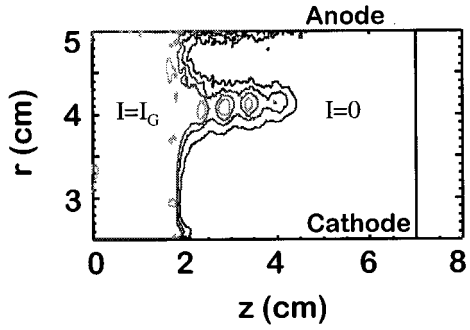

FIG. 3. Current enclosed contours ($I=-2\pi rB_\theta/\mu_0=$constant) at $t=2$ ns in negative polarity for the parabolic density profile. The contours are normalized so that the units are kA with $I_G=20$ kA and an interval of 4 kA between contour levels.

rapid magnetic field penetration takes place at a radial position where the maximum Hall speed occurs and no magnetic field penetration takes place in regions where the Hall speed is negative. Simulation results (not shown) also show that the regions of penetration and exclusion are reversed in positive polarity. However, the penetration speed predicted by the PIC method is about 50% slower than predicted by fluid theory. A one-dimensional analysis of Eq. (4) indicates that electron inertia does not change the penetration speed.[28] Therefore, it is speculated that the slower penetration is caused by either strong two-dimensional effects or by the effects of electron pressure that are not included in the fluid analysis.

Figure 4 shows the current enclosed contours for the uniform-parabolic density profile in positive polarity. As predicted by theory, no magnetic field penetration into the bulk plasma deeper than a collisionless skin depth is observed. Rapid penetration of magnetic field is observed at the anode in both Figs. 3 and 4. Anode penetration occurs because the conductor boundary condition ($E_\parallel=0$) causes electrons to $\mathbf{E}\times\mathbf{B}$ drift parallel to the anode.[29] Therefore, this penetration is strongly coupled to the anode boundary conditions and is different from the Hall penetration observed in the body of the plasma.

Figure 3 also shows that magnetic field penetration is accompanied by a train of vortices in the electron flow. The

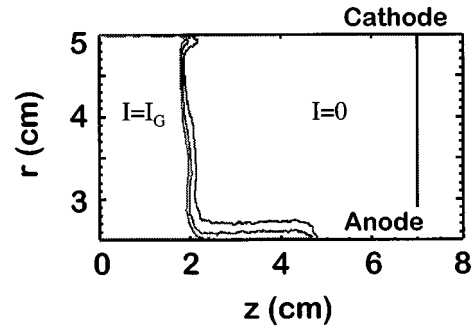

FIG. 4. Current enclosed contours ($I=2\pi rB_\theta/\mu_0=$constant) at $t=2$ ns in positive polarity for the uniform-parabolic density profile. The contours are normalized so that the units are kA with $I_G=20$ kA and an interval of 4 kA between contour levels.

radius of the vortices is about 0.25 cm which is comparable to both the characteristic Hall scale length (L_H) and the collisionless skin depth (c/ω_{pe}). Magnetic flux is compressed inside each vortex producing eddy currents in the center that are larger than the drive current. A one-dimensional analysis of Eq. (4) predicts oscillations in the magnetic field behind the shock front that can also be larger than the drive field.[28] The wavelength of these oscillations is proportional to the collisionless electron skin depth.

The center of a vortex is charged positively which is produced by a reduction in the number of electrons in the center of the vortex. This space charge imbalance produces an electric field that allows the electrons to $\mathbf{E}\times\mathbf{B}$ drift in a counterclockwise direction around the positively charged center. The detailed electron dynamics inside a vortex is beyond the scope of this paper. However, since the vortices are observed to be paramagnetic, the conservation of generalized vorticity prohibits the vortices from being comprised entirely of electrons from the plasma prefill when pressure and collision terms are neglected in Eq. (4). To see this assume that the pressure term can be neglected so that $\Gamma=0$ for the electrons in the plasma prefill. For these electrons

$$(\nabla\times\gamma V_e)_\theta=\Omega_\theta. \tag{11}$$

If Eq. (11) is integrated across the area of a vortex then it is possible to write

$$R\gamma(R)V_\varphi(R)=\int_0^R \Omega_\theta R'\,dR', \tag{12}$$

where R is the vortex radius, and φ is the coordinate direction around the vortex. Since $\Omega_\theta<0$ in these simulations, Eq. (12) predicts that $V_\varphi<0$. This direction of rotation is such as to produce diamagnetic vortices. However, the vortices are observed to be paramagnetic which implies that our assumption that the pressure term is negligible and the vortices contain only electrons from the initial plasma prefill is false. Therefore, either the pressure terms are important or the vortices must contain a sufficient number of emitted electrons with positive initial generalized vorticity. These issues will be investigated in a future paper.

To better understand the role of ion motion, a simulation was run with the parabolic density profile in negative polarity and an ion mass 1/4 the proton mass. For this choice of parameters, $c/\omega_{pi}=8$ cm at the radial position where the most rapid penetration of magnetic field is expected. Because $c/\omega_{pi}\gg L_H$ the simulation is still in a regime where Hall penetration is expected to dominate. The current enclosed contours at $t=2$ ns are shown in Fig. 5. Figure 5 demonstrates that, when ions can move, the vortices exhibit a smaller degree of paramagnetism than the infinitely massive case shown in Fig. 3. In the simulations depicted in Fig. 3, the maximum electric field in a vortex at $t=2$ ns is 250 kV/cm. This electric field is sufficient to move ions several mm in this time and thus significantly reduces the space charge imbalance necessary to support the vortices. Magnetic field penetration followed by the removal of ions due to the electrostatic forces has been shown to lead to gap opening in a POS.[17] The details of this process and the role of the Hall electric field will be the subject of a future paper.

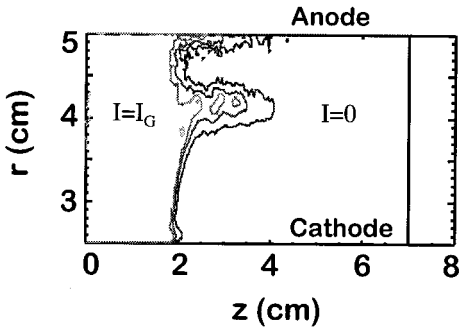

FIG. 5. Current enclosed contours ($I=-2\pi rB_\theta/\mu_0=$constant) at $t=2$ ns in negative polarity for a case where ions can move ($c/\omega_{pi}=8$ cm) with the parabolic density profile. The contours are normalized so that the units are kA with $I_G=20$ kA and an interval of 4 kA between contour levels.

As mentioned above, the size (radius) of the vortices in Fig. 3 is comparable to both the collisionless skin depth and the characteristic Hall scale length. It is of interest to understand whether the vortex size scales with the characteristic Hall scale length, L_H, or the collisionless electron skin depth, c/ω_{pe}. To examine this question, a simulation was run with a density profile for which the Hall speed is independent of r. This profile is given by

$$n(r)=\frac{n_c r_c^2}{r^2}\,\frac{1}{1-f\,\ln(r/r_c)}, \tag{13}$$

where $0<f<1/\ln(r_a/r_c)$ is a parameter that sets the Hall speed. The penetration speed for the density distribution given by Eq. (13) can be written as

$$V_H=\alpha\,\frac{c(-r_cB_c)}{4\pi n_c e r_c^2}\,f, \tag{14}$$

where α is defined in the text following Eq. (9). The solid curve in Fig. 6 shows the density profile for $f=1/2$, $r_c=1$ cm, $r_a=5$ cm, and $n_c=5\times10^{12}$ cm^{-3}. For this choice of parameters the characteristic Hall scale length is about 2 cm while the collisionless electron skin depth is about 0.3 cm. The density profile used in the simulations is given by the dashed curve in Fig. 6 which shows a slightly modified density distribution near the cathode. This slightly altered profile was chosen to avoid problems associated with magnetic field penetration right at the cathode boundary. Since $d(Znr^2)/dr<0$ near the cathode, field penetration is not expected there. The simulations for the density profile shown in Fig. 6 were done in negative polarity with an electron mass 1/90 the normal electron mass. The applied current rose from 0 to 5 kA in approximately 1.5 ns and then was held constant.

The current enclosed contours at $t=5$ ns and $t=10$ ns from a simulation with the density profile depicted in Fig. 6 are shown in Fig. 7. The current enclosed contours at $t=5$ ns [Fig. 7(a)] show the formation of a line of vortices along the plasma/magnetic field boundary. Each of these vortices has a diameter of about two collisionless electron skin depths. These results show that the vortex size scales with c/ω_{pe} and not L_H. The penetration speed in this simulation is only 10% slower than that predicted by fluid theory. The current en-

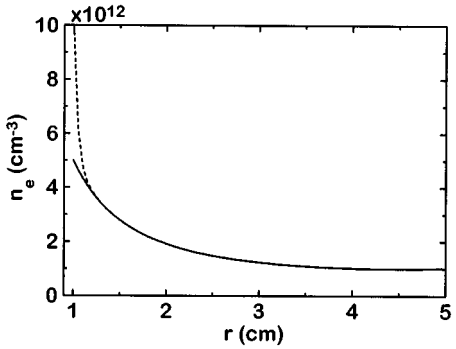

FIG. 6. The density profile for which the Hall speed is independent of r. The solid curve is the density profile described by Eq. (13). A slightly modified version of this profile near the cathode given by the dashed curve was used in the simulations.

closed contours at $t=10$ ns [Fig. 7(b)] show that this initial line of vortices propagates into the plasma at approximately the same axial speed. As the initial line of vortices propagates into the plasma, additional lines of weaker vortices form along the plasma/magnetic field boundary. Each line of the additional lines of vortices propagates with the same axial speed as the initial line of vortices but exhibit a smaller degree of paramagnetism. Notice that the vortices drift slightly radially upward as they propagate into the plasma. This radial drift may be caused by either interactions with other vortices or by interactions with a boundary.

The simulations presented thus far have been with an electron density that is much smaller than those expected in a real POS. This density was chosen to keep the numerical plasma temperature as low as possible. In addition, the electron mass was reduced to keep the electron collisionless skin depth small compared to the size of the plasma. In the remainder of this section it is demonstrated that the simulations with reduced density, magnetic field, and electron mass are essentially equivalent to simulations with normal electron mass with density and magnetic field increased by $\kappa=m_e/m$ where m is the artificially light electron mass. That this is true can be seen by multiplying Eqs. (1)–(3) and Ampère's law by $1/\kappa$. These new equations describe the dynamics of a species with mass $m=m_e/\kappa$. The dynamics of this new species is unchanged provided the drive magnetic field and density are scaled by the factor $1/\kappa$.

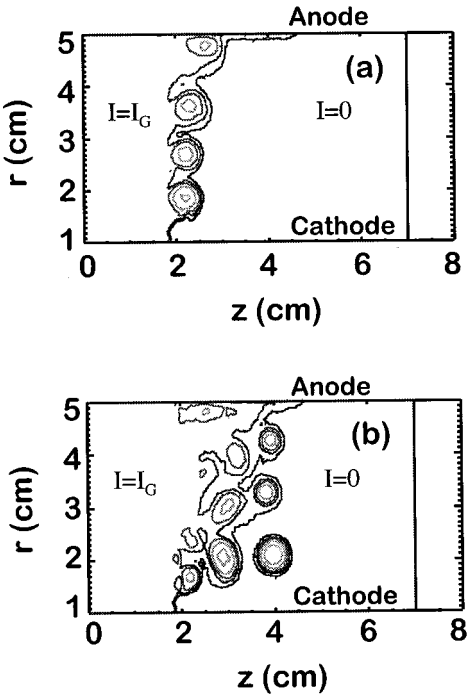

FIG. 7. Current enclosed contours ($I=-2\pi rB_\theta/\mu_0=$constant) at (a) $t=5$ ns and (b) $t=10$ ns in negative polarity for the density profile depicted in Fig. 6. The contours are normalized so that the units are kA with $I_G=5$ kA and an interval of 1 kA between contour levels.

The relative importance of the numerical plasma heating can be estimated by comparing the electron velocity in the current channel with the thermal speed. To first order the electron speed in the current channel can be estimated from Ampère's law to be

$$|V_e|=\frac{c}{4\pi en_e}|\nabla\times B|\cong\frac{c|B|}{4\pi en_e}\frac{\omega_{pe}}{c}, \tag{15}$$

where it has been assumed that the width of the current channel in the plasma is c/ω_{pe}. The ratio of the electron speed in the current channel to the electron thermal speed $[V_{\rm th}=(2k_{\rm B}T/m_e)^{1/2}]$ can be written as

$$V_{\rm th}/V_e=\left(\frac{n_ek_{\rm B}T}{B^2/8\pi}\right)^{1/2}. \tag{16}$$

Equation (16) shows that the relative importance of numerical plasma heating is small provided the ratio of kinetic pressure to magnetic pressure is small. It is important to note that, for a fixed grid, the numerical temperature is proportional to the density [see Eq. (10)]. Therefore, the relative importance of numerical plasma heating is unchanged if B and n_e are increased by the same factor.

To test these ideas a simulation was run with the density profile given by Eq. (13) using normal electron mass, $n_c=4.5\times10^{14}$ cm^{-3}, and $I_G=450$ kA. This simulation should be similar to the simulation with $m=m_e/90$, $n_c=5\times10^{12}$ cm^{-3}, and $I_G=5$ kA shown in Fig. 7. Current enclosed contours for this simulation at $t=5$ and 10 ns are shown in Fig. 8. Although there are minor differences between the simulation results depicted in Figs. 7 and 8, the size of the vortices and the speed of penetration remain unchanged. This shows that the simulations with reduced electron mass are essentially equivalent to simulations with normal electron mass with a corresponding higher density and magnetic field.

IV. ENERGY CONSIDERATIONS

It is of considerable interest to investigate the flow of energy as the magnetic field penetrates into the plasma. For the simulations described in this paper, conservation of energy over the plasma volume can be expressed as

$$E_{\rm IN}=E_B+E_E+E_P+E_A, \tag{17}$$

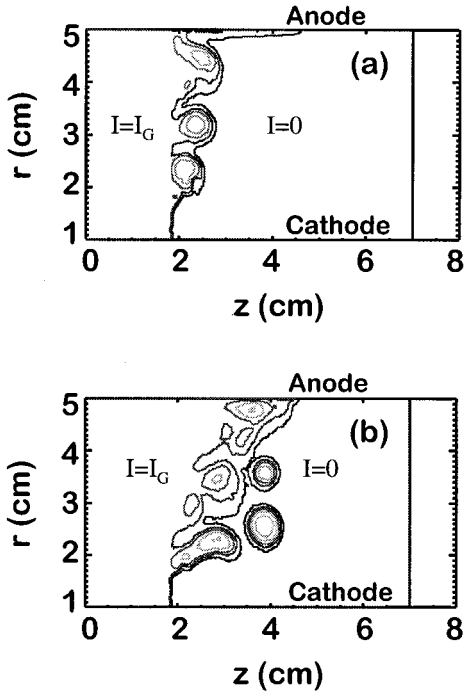

FIG. 8. Current enclosed contours ($I=-2\pi rB_\theta/\mu_0$=constant) at (a) $t=5$ ns and (b) $t=10$ ns in negative polarity for the density profile given by Eq. (13). These results are for normal electron mass with the density and applied magnetic field scaled up by a factor of 90 over that used in obtaining the results shown in Fig. 7. The contours are normalized so that the units are kA with $I_G=450$ kA and an interval of 90 kA between contour levels.

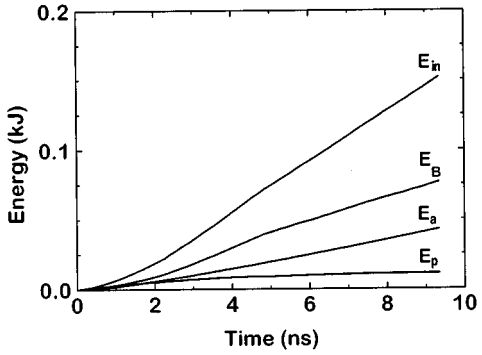

FIG. 9. The partition of energy in the plasma for the simulation shown in Fig. 7. The energy flowing into the plasma is $E_{\rm in}$, the magnetic energy is E_B, the energy convected to the boundary by electrons is E_A, and the internal plasma energy is E_p.

where $E_{\rm IN}=(c/4\pi)\int dt\int \mathbf{E}\times\mathbf{B}\cdot\hat{n}dA$ is the energy flowing into the plasma through the generator boundary, $E_B=\int(B^2/8\pi)d^3x$ is the magnetic-field energy, $E_E=\int(E^2/8\pi)d^3x$ is the electric-field energy, $E_P=\Sigma_{i=1}^{N_p}(\gamma_i-1)mc^2$ is the total internal energy of the plasma, $E_A=\Sigma_{i=1}^{N_{\rm A}}(\gamma_i-1)mc^2$ is the particle energy that flows out through the anode, N_p is the number of plasma particles in the simulation at time t, and $N_{\rm A}$ is the total number of particles leaving the volume through the boundaries. For the simulations described here, the energy flow out of the plasma occurs by the electrons in the current channel that flow to the anode. Terms describing the flow of electromagnetic energy out of the plasma and the flow of particle energy into the plasma from the cathode have been omitted in Eq. (17) since the simulations show that these terms are negligible.

For an applied current that is constant in time the Hall model predicts that the rate at which energy flows into the plasma is[30]

$$\frac{dE_{\rm IN}}{dt}=\frac{c}{2}\int E_rB_\theta r\,dr=\frac{cr_cB_c(t)}{16\pi Zen_e}\left(1-\frac{n_cr_c^2}{n_ar_a^2}\right). \qquad (18)$$

It can also be shown from fluid theory that half the energy that flows into the plasma goes into magnetic field energy.[31] The other half of the energy that flows into the plasma is either dissipated in the plasma or flows out of the plasma to the boundaries. In Ref. 31 it was shown that, if there is a small amount of resistivity, electrons are heated in the shock front where large magnetic field gradients exist. In this case the dissipated energy stays in the plasma and goes into electron thermal motion. For the parameters expected in a POS, this picture would lead to unrealistically large electron temperatures. Therefore, it is likely that a large fraction of the energy is convected out of the plasma to the anode by the electrons in the current channel.[32,33] In addition to plasma heating and convection to the anode, the simulation results shown in Figs. 3, 7, and 8 show that energy can also go into the electron vortex motion (i.e., the kinetic energy associated with the electron rotation around the center of a vortex).

The partition of energy for the simulation depicted in Fig. 7 is shown in Fig. 9. It is well known that PIC codes do not exactly conserve energy.[11] In this simulation great care was taken so that energy conservation was obeyed to within 10%. As Fig. 9 shows, nearly half the energy that flows into the plasma goes into magnetic field energy. The majority of the remaining energy is convected to the anode by the electrons in the current channel. However, Fig. 9 also shows that a significant amount of energy goes into increasing the internal plasma energy. The internal plasma energy appears primarily in the form of vortices. The internal plasma energy initially rises rapidly as the initial line of vortices is created but increases much more slowly once the initial vortices are established. Once the initial line of vortices is established, the rate at which energy is convected to the anode is about the same as the rate at which magnetic energy increases in the plasma. The electric field energy is not shown in Fig. 9 since the simulations show it is much smaller than both the magnetic field energy and the internal energy of the plasma. In Sec. III it was shown that large electrostatic electric fields exist inside a vortex. However, the total electrostatic energy associated with this field is small because $|\mathbf{E}|/|\mathbf{B}|\sim|\mathbf{V}_e|/c<1$ inside a vortex and the electric field is confined to this region which occupies only a small fraction of the entire plasma volume.

V. CONCLUSIONS

This paper has used a PIC code to demonstrate fast magnetic field penetration into a plasma associated with the Hall term in fluid theory. This is an improvement over traditional fluid treatments since the PIC method makes no *a priori* assumptions about the plasma equation of state, form of the

pressure tensor, or the importance of displacement currents. In addition, fluid treatments generally require a small amount of collisionality to remove singularities in the solutions. Since the PIC technique is inherently collisionless, the PIC results described in this paper treat the collisionless transport of magnetic field into the plasma.

The simulations reproduce many aspects of magnetic field penetration that are consistent with fluid treatments. However, the speed of penetration observed in the simulations is somewhat slower than analytic estimates. This is caused by either strong two-dimensional effects or by the effects of the pressure tensor ignored in the fluid analysis. The simulations show the formation of vortices behind the EMHD shock front that are a natural consequence of electron inertia. These vortices are paramagnetic in nature and their size is a few collisionless electron skin depths.

Most of the results described in this paper are for the case of infinitely massive ions. When ions can move, axial magnetic field penetration is followed by ion motion produced by the large electrostatic force that exists in the center of a vortex. In this case, the vortices in the electron flow are much weaker since the ion motion acts to reduce the space charge separation that is necessary to support the vortices. The reduction of ion space charge in regions where the magnetic field penetrates may also lead to gap formation in a POS.

It is observed that half the energy flowing into the plasma goes into magnetic energy. The majority of the remaining energy is convected to the anode by the electrons in the current channel. A significant amount of energy also goes into the internal energy of the plasma while the initial line of vortices is being established. However, once the initial line of vortices is created, very little additional energy appears as internal plasma energy and the rate at which energy is convected to the anode is approximately the same as the rate of increase in the magnetic field energy in the plasma.

ACKNOWLEDGMENTS

The authors would like to acknowledge Dr. Joe Huba of the Naval Research Laboratory (NRL) for many interesting discussions pertaining to this problem. In addition, many thanks to Dr. Bob Commisso and Dr. Bruce Weber at NRL for their continued interest in this work. The authors also profited greatly from the careful reading and technical discussions of this manuscript provided by David Rose. S.B.S. also benefited from discussions with Dr. Larry (Lars) Ludeking and Dr. David Smithe of Mission Research Corporation. Simulation results were obtained using the MAGIC code under the Air Force Office of Scientific Research sponsored MAGIC User's Group.

This work was supported by the Defense Nuclear Agency.

[1] R. J. Commisso, P. J. Goodrich, J. M. Grossmann, D. D. Hinshelwood, P. F. Ottinger, and B. V. Weber, Phys. Fluids B **4**, 2368 (1992).
[2] See IEEE Trans. Plasma Sci. **PS-15** (1987), special issue on Plasma Opening Switches.
[3] P. A. Bernhardt, Phys. Fluids B **4**, 2249 (1992).
[4] P. Sheehey, J. E. Hammel, I. R. Lindemuth, D. W. Scudder, J. S. Schlachter, R. H. Lovberg, and R. A. Riley, Phys. Fluids B **4**, 3698 (1992).
[5] A. Fruchtman and Y. Maron, Phys. Fluids B **3**, 1546 (1991).
[6] K. Gomberoff and A. Fruchtman, Phys. Plasmas **1**, 2480 (1994).
[7] R. L. Stenzel, J. M. Urrutia, and C. L. Rousculp, Phys. Rev. Lett. **74**, 702 (1995).
[8] M. Rosenbluth, in *Plasma Physics and Thermonuclear Research*, edited by C. L. Longmire, J. L. Tuck, and W. B. Thompson (Pergamon, London, 1963), p. 217.
[9] J. D. Jackson, *Classical Electrodynamics* (Wiley, New York, 1975), pp. 472 and 473.
[10] A. S. Kingsep, K. V. Chukbar, and V. V. Yankov, in *Reviews of Plasma Physics*, edited by B. B. Kadomstev (Consultants Bureau, New York, 1990), Vol. 16, p. 243.
[11] C. K. Birdsall and A. B. Langdon, *Plasma Physics via Computer Simulation* (McGraw-Hill, New York, 1985), p. 179.
[12] B. Goplen, L. Ludeking, D. Smithe, and G. Warren, Comput Phys. Commun. **87**, 54 (1995).
[13] A. S. Kingsep, L. I. Rudakov, and K. V. Chukbar, Sov. Phys. Dokl. **27**, 140 (1982).
[14] A. S. Kingsep, Y. V. Mokhov, and K. V. Chukbar, Sov. J. Plasma Phys. **10**, 495 (1984).
[15] A. Fruchtman, Phys. Fluids B **3**, 1908 (1991).
[16] J. D. Huba, J. M. Grossmann, and P. F. Ottinger, Phys. Plasmas **1**, 3444 (1994).
[17] See National Technical Information Service Document No. PB95-14437 (J. M. Grossmann, S. B. Swanekamp, R. J. Commisso, P. J. Goodrich, D. D. Hinshelwood, J. D. Huba, P. F. Ottinger, and B. V. Weber, Proceedings of the 10th International Conference on High Power Particle Beams, edited by W. Rix and R. White, San Diego, CA, 20–24 June 1994, p. 280). Copies can be ordered from the National Technical Information Service Springfield, VA 22151.
[18] L. I. Rudakov, C. E. Seyler, and R. N. Sudan, Comments Plasma Phys. Controlled Fusion **14**, 171 (1991).
[19] P. M. Bellan, Phys. Fluids B **5**, 1955 (1993).
[20] M. B. Isichenko and A. M. Marnachev, Sov. Phys. JETP **66**, 702 (1987).
[21] A. Fruchtman and K. Gomberoff, Phys. Fluids B **5**, 2371 (1993).
[22] R. J. Mason, P. L. Auer, R. N. Sudan, B. V. Oliver, C. E. Seyler, and J. B. Greenly, Phys. Fluids B **5**, 1115 (1993).
[23] B. Church and R. N. Sudan, Phys. Plasmas **2**, 1837 (1995).
[24] D. Mosher (private communication).
[25] R. Kulsrud, P. F. Ottinger, and J. M. Grossmann, Phys. Fluids **31**, 1741 (1988).
[26] K. Gomberoff and A. Fruchtman, Phys. Fluids B **5**, 2841 (1993).
[27] B. V. Weber, R. J. Commisso, P. J. Goodrich, J. M. Grossmann, D. D. Hinshelwood, P. F. Ottinger, and S. B. Swanekamp, Phys. Plasmas **2**, 299 (1995).
[28] Y. L. Kalda and A. S. Kingsep, Sov. J. Plasma Phys. **15**, 508 (1989).
[29] J. M. Grossmann, S. B. Swanekamp, P. F. Ottinger, R. J. Commisso, D. D. Hinshelwood, and B. V. Weber, Phys. Plasmas **2**, 299 (1995).
[30] A. Fruchtman, Phys. Rev. A **45**, 3938 (1992).
[31] A. Fruchtman and K. Gomberoff, Phys. Fluids B **4**, 117 (1992).
[32] A. Fruchtman and L. I. Rudakov, Phys. Rev. E **50**, 2997 (1994).
[33] J. M. Grossmann, P. F. Ottinger, and R. J. Mason, J. Appl. Phys. **16**, 2307 (1989).